Supporting Information

Savolainen et al. 10.1073/pnas.1317459110

SI Text

Fig. S1*A* shows the terahertz (THz) pulse in time and in frequency domain (*Inset*) and Fig. S1*B* an autocorrelation of the Raman pump pulse.

Fig. S2*A* shows a 1D cut along t_1 when increasing the Raman-pump intensity beyond the threshold for the generation of a solvated electron. Fig. S2*B* shows the polarization dependence of the 2D Raman-THz signal for 1D cut along t_1 with the Raman-pump intensity below that threshold.

SI Materials and Methods

Transfer Functions and Pulses. The calculation of the detected signal from a molecular response function $R(t',t'')$ using Eqs. **1** and **3** requires the precise knowledge of the input THz field E_{THz}, as well as the propagation effects for the emitted third-order field to the detection crystal (1). The latter is described on the level of a linear transfer function in the frequency domain $T_{total}(\omega)$. The schematic Fig. S3 shows that this total transfer function $T_{total}(\omega)$ includes contributions from the water jet $T_{water}(\omega)$, from the imaging optics $T_{image}(\omega)$, and the detection crystal $T_{crystal}(\omega)$. The experimental determination of all transfer functions as well as of the input THz field E_{THz} will be discussed below. The 800-nm Raman pump pulse I_{Raman}, which also enters Eq. **1**, experiences only negligible dispersion and absorption in the thin water jet, and has been modeled as a Gaussian pulse with FWHM of 110 fs (Fig. 1*B*).

The transfer function $T_{water}(\omega)$ can be determined experimentally by measuring the pulses transmitted through the whole setup with and without water jet, revealing E_{II} (Fig. S4*B*) and E_{I} (Fig. S4*A*), respectively:

$$T_{water}(\omega)=\frac{E_{\mathrm{II}}(\omega)}{E_{\mathrm{I}}(\omega)}. \qquad \textbf{[S1]}$$

The temporal shift of the pulse peak due to the index of refraction of water, resulting in a linear spectral phase, has been removed before Fourier transforming $E_{\mathrm{II}}(t)$ and $E_{\mathrm{I}}(t)$. As a good approximation of propagation effects within the water jet, we assume that the input THz pulse interacts in the middle of the water jet after propagating through its first half, and likewise, the emitted field is generated in the middle of the jet and propagates through the second half. Hence, one part of the water transfer function, modeled as $\sqrt{T_{water}(\omega)}$, will contribute to the input THz pulse (see Eq. **S5** below), and the second part $\sqrt{T_{water}(\omega)}$ to $T_{total}(\omega)$ (see Eq. **S4** below). A more accurate description of propagation effects of the interaction in the water jet would require a split-step Fourier method that models the water jet as even smaller slices, but because the water jet is already quite thin (40 μm), the present approximation is believed to capture the essence of the propagation effect well enough.

Subsequently, the emitted signal propagates from the sample position to the detection position experiencing $T_{image}(\omega)$, which can be determined by moving the detection crystal precisely at the sample position and measuring the THz field there (E_{III}, Fig. S4*C*), and then comparing it to the THz field measured at the detection crystal position (E_{I}, Fig. S4*A*):

$$T_{image}(\omega)=\frac{E_{\mathrm{I}}(\omega)}{E_{\mathrm{III}}(\omega)}. \qquad \textbf{[S2]}$$

Due to the high-aperture optics used, this transfer function is quite flat down to 0.3 THz.

Determining $T_{crystal}(\omega)$ is less straightforward. To obtain this transfer function, we generated a THz pulse at the sample position by moving the generation crystal, and by reducing the pump intensity dramatically to about 100 nJ, so that saturation effects in the generation process can be neglected. In that case, the emitted field would just be the first derivative of the generating pulse (a Gaussian pulse with 110-fs FWHM; Fig. S1*B*), if the generation crystal were free of dispersion and absorption (1–3). The measured field E_{IV} (Fig. S4*D*) is thus compared with such an idealized pulse E_{V} (Fig. S4*E*). In addition, we have to remove the effect of $T_{image}(\omega)$ from that measurement, so that we obtain for $T_{crystal}(\omega)$

$$T_{crystal}(\omega)=\frac{E_{\mathrm{IV}}(\omega)}{E_{\mathrm{V}}(\omega)}\cdot\frac{1}{T_{image}(\omega)}. \qquad \textbf{[S3]}$$

That procedure reveals the combined effect of both the generation and detection crystals. As we use identical crystals for both, we assume that $\sqrt{T_{crystal}(\omega)}$ describes the detection process and thus contributes to the total transfer function. With these ingredients, the total transfer function becomes

$$T_{total}(\omega)=\sqrt{T_{water}(\omega)}\cdot T_{image}(\omega)\cdot\sqrt{T_{crystal}(\omega)}. \qquad \textbf{[S4]}$$

All of the resulting transfer functions obtained from Eqs. **S1**–**S4** are presented in Fig. S5.

With the known transfer functions, we can also calculate the input THz pulse $E_{THz}(t)$ in the middle of the water jet, which enters Eq. **1**. To that end, we start from the pulse E_{III} measured at the sample position without water jet, propagate it through half the water jet, and take out the effect of the detection crystal (Fig. S4*F*, gray line):

$$E_{THz}(\omega)=E_{\mathrm{III}}(\omega)\frac{\sqrt{T_{water}(\omega)}}{\sqrt{T_{crystal}(\omega)}}. \qquad \textbf{[S5]}$$

The measurement of the transfer functions is noisy in regions where the spectral intensity of the pulses is low, i.e., below ~0.3 THz and above ~6 THz. We therefore fitted, and effectively extrapolated to zero and toward higher frequencies, the total transfer function T_{total} from Eq. **4**. We used a phenomenological function:

$$|T_{total}(\omega)|\propto(1-e^{-\omega/\omega_1})\frac{\omega_2^2}{\omega^2+\omega_2^2} \qquad \textbf{[S6]}$$

for the amplitude, revealing $\omega_1=1.4$ THz and $\omega_2=1.9$ THz. The phase was fitted to a quadratic function:

$$\arg(T_{total}(\omega))=\phi_0+d\phi(\omega-\omega_0)^2, \qquad \textbf{[S7]}$$

with $\phi_0=0.25$, $d\phi_0=-0.073$, and $\omega_0=1.0$ THz. The fits are shown in Fig. S4*D* (gray lines). Similarly, the transfer function in Eq. **S5** was fit to a phenomenological function:

$$\left|\frac{\sqrt{T_{water}(\omega)}}{\sqrt{T_{crystal}(\omega)}}\right|\propto a_1e^{-\omega/\omega_1'}+e^{-\omega/\omega_2'}, \qquad \textbf{[S8]}$$

revealing $\omega_1'=0.23$ THz, $a_1=5$, $\omega_2'=7.2$ THz, and again to a quadratic function for the phase with $\phi_0'=0.24$, $d\phi_0'=-0.13$, and $\omega_0'=1.9$ THz.

Control of the Gouy Phase Shift. In the construction of the instrument response function, we must consider the well-known effect of the Gouy phase shift that varies the phase of a pulse when it passes through a focus (4–7). Unlike in conventional nonlinear spectroscopy, where many-cycle pulses are most commonly used, the absolute phase of the THz field in Eq. **1** in fact matters in 2D Raman-THz spectroscopy with half-cycle THz pulses. That is, the accumulated Gouy phase shift in the input THz field $E_{THz}(t)$ before the sample does not cancel out in the signal propagation after the sample (this effect will be discussed in detail in a separate publication). The Gouy phase modulates the THz field on a scale that equals the Rayleigh length, which in our case is of the order of only a few hundreds of micrometers because we use a small focus with high numerical aperture optics to achieve field amplitudes as high as possible. Consequently, the positioning of the crystals and the sample is critical within ~100 μm. In the present work, we take care of the Gouy phase shift by precisely positioning the water jet and the crystals in the foci of the imaging optics.

The two elliptical mirrors were machined and mounted (without possibility of further alignment) in a way that we know the position of their foci with the help of an additionally designed alignment tool (i.e., a thin Al plate with a small pinhole of ~200 μm positioned on a magnetic retention base). The estimated error in the positioning of the mirrors and the alignment tools is on the order of 100 μm. Further uncertainties originate from the additional optical path lengths introduced by the generation and detection crystals, both with thickness $d = 100$ μm and index of refraction of $n \sim 3$, which amounts to a shift of foci of $d(n-1) = 200$ μm in either case. As a starting point, we assumed that the nonlinear processes happen effectively in the middle of the crystals, but that assumption is weak in particular for the THz generation process, for which the GaP crystal is strongly pumped so that depletion effects due to two-photon absorption can no longer be neglected. The effect of the water jet ($d = 40$ μm, $n = 2$) on the optical path length is negligible.

With these uncertainties in mind, we positioned the crystals and the water jet in the following way. We first placed generation and detection crystals precisely at their predetermined foci using the alignment tool together with a confocal sensor (ConfocalDT, microepsilon, resolution ~5 μm). The positioning was then optimized by observing the Gouy phase at the detection crystal position and trying to get a pulse $E_{\mathrm{I}}(t)$ as symmetric as possible (Fig. S4*A*), resulting in a shift of the latter of ~130 μm toward the elliptical mirror, which is consistent with the effect of the additional optical path length introduced by both crystals. The detection crystal was subsequently moved to the sample position at its predetermined focus, where the pulse entering the sample $E_{\mathrm{III}}(t)$ (Fig. S4*C*) was measured. The pulse is slightly asymmetric, in contrast with $E_{\mathrm{I}}(t)$ (Fig. S4*A*), whose Gouy phase has been optimized, and we assume the asymmetry to be the result of the combined uncertainties in the determination of the positions of the foci. We therefore allowed for a small correcting phase ϕ for the input THz pulse and replaced Eq. **S5** by

$$E_{THz}(\omega) = e^{i\phi} E_{\mathrm{III}}(\omega) \frac{\sqrt{T_{water}(\omega)}}{\sqrt{T_{crystal}(\omega)}}. \qquad \textbf{[S9]}$$

The resulting pulse is shown in Fig. S4*F*, black line. We also added a compensating phase to the emitted field:

$$T_{total}(\omega) = e^{-i\phi} \sqrt{T_{water}(\omega)} \cdot T_{image}(\omega) \cdot \sqrt{T_{crystal}(\omega)}. \qquad \textbf{[S10]}$$

The value of that phase, $\phi = 0.4$, has been determined by matching the antidiagonal ridge of the instrument response function (IRF) and the amplitude ratio of its positive and negative peaks around $t_1 = t_2 = 0$ (Fig. 2*C*) to the corresponding features I and II in the experimental data (Fig. 2*B*). We thereby assumed that these features originate from an essentially instantaneous part of the water response function such as from the electronic polarizability or the librational modes of water. We independently measured that a Gouy phase of $\phi = 0.4$ corresponds to a shift of the foci of 150 μm, which is well within the uncertainty of our alignment procedure. Note that even substantially larger phase corrections have no effect on the comparison shown in Fig. 4; the diagonal decay of the experimental data will always remain significantly slower than that of the IRF.

1. Němec H, Kadlec K, Kužel P (2002) Methodology of an optical pump-terahertz probe experiment: An analytical frequency domain approach. *J Chem Phys* 117(18):8454–8466.
2. Faure J, van Tilborg J, Kaindl RA, Leemans WP (2004) Modelling laser based table-top THz sources: Optical rectification, propagation and electro-optic sampling. *Opt Quantum Electron* 36:681–697.
3. Kindt JT, Schmuttenmaer CA (1999) Theory for determination of the low-frequency time-dependent response function in liquids using time-resolved terahertz pulse spectroscopy. *J Chem Phys* 110(17):8589–8596.
4. Feng S, Winful HG, Hellwarth RW (1998) Gouy shift and temporal reshaping of focused single-cycle electromagnetic pulses. *Opt Lett* 23(5):385–387.
5. Kužel P, Khazan MA, Kroupa J (1999) Spatiotemporal transformations of ultrashort terahertz pulses. *J Opt Soc Am B* 16:1795–1800.
6. Ruffin AB, Rudd JV, Whitaker JF, Feng S, Winful HG (1999) Direct observation of the Gouy phase shift with single-cycle terahertz pulses. *Phys Rev Lett* 83(17):3410–3413.
7. Feurer T, Stoyanov NS, Ward DW, Nelson KA (2002) Direct visualization of the Gouy phase by focusing phonon polaritons. *Phys Rev Lett* 88(25):257402.

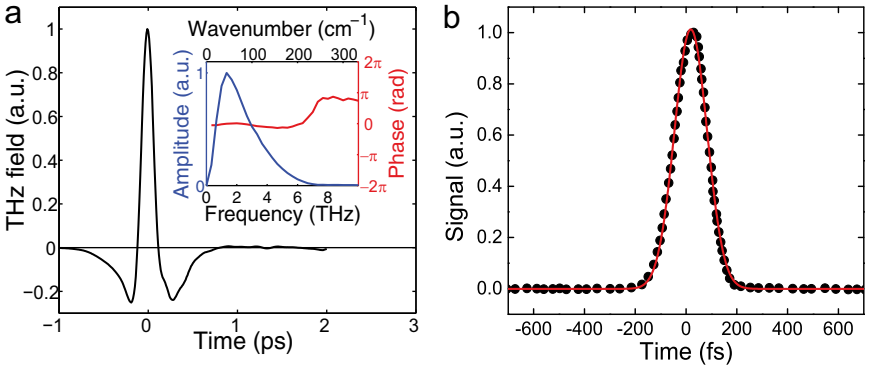

Fig. S1. (*A*) THz pulse in time domain. (*Inset*) Amplitude and phase in frequency domain. (*B*) Raman pulse autocorrelation (black dots) and Gaussian fit (red line).

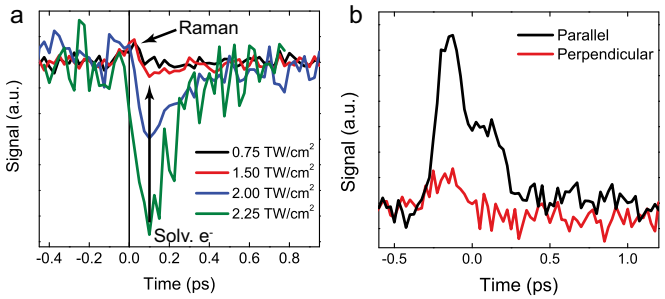

Fig. S2. Verifying the origin of the 2D Raman-THz signal. (*A*) The emerging Raman-induced signal and the vanishing solvated electron signal with decreasing Raman pulse fluency. (*B*) The dependency of the 2D Raman-THz signal on the polarization between the Raman and THz pulses. The transfer functions and the setting of the Gouy phase in these measurements were different from Fig. 2, but the data within one measurement series are self-consistent.

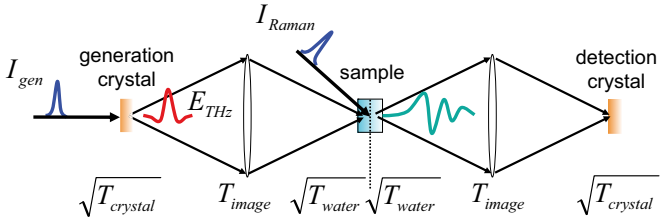

Fig. S3. Two-dimensional Raman-THz experimental scheme. Shown are the generated THz field (red), Raman pump pulse (blue), and the emitted field (green). Also shown are the transfer functions that describe the propagation effects in the sample (T_{water}), for either one of the imaging optics (T_{image}), and the combined effects of generation and detection in the crystals ($T_{crystal}$).

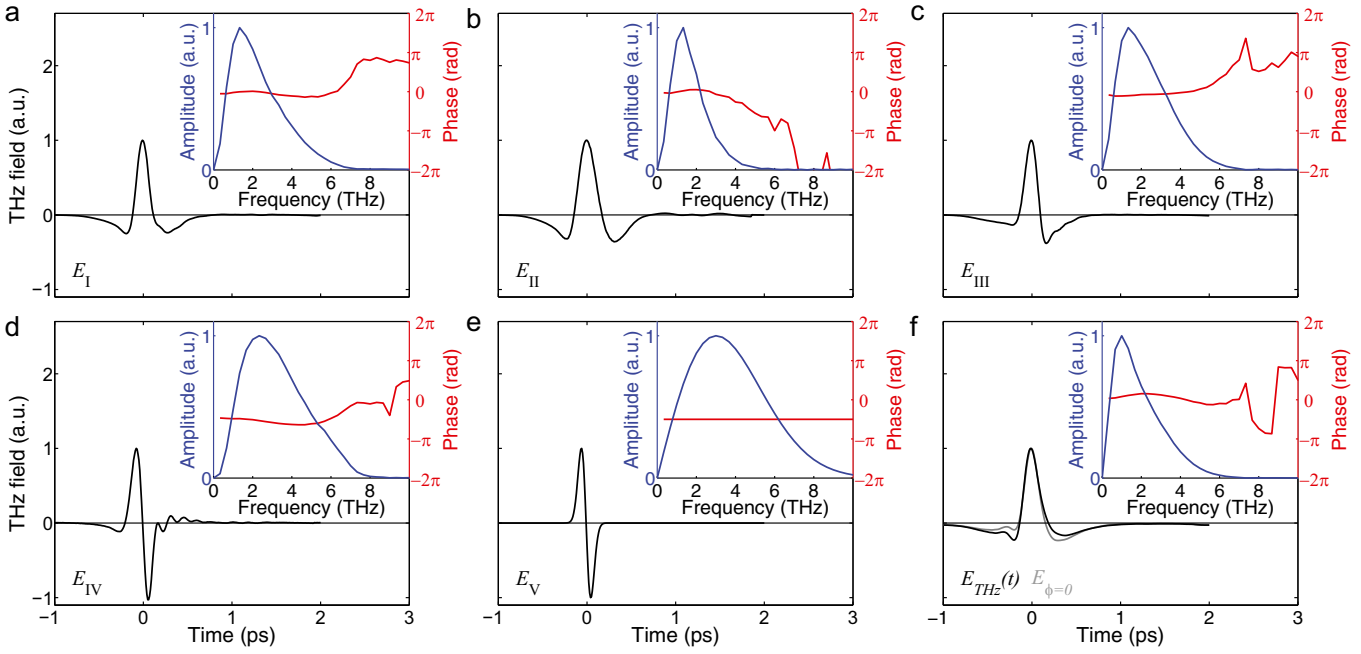

Fig. S4. (*Insets*) Electric fields of the THz pulses in time and frequency domain. (*A*) E_{I}, pulse measured at detection position. (*B*) E_{II}, pulse measured at detection position having the water sample in the beam. (*C*) E_{III}, pulse measured at the sample position. (*D*) E_{IV}, pulse created at the sample position with low energy. (*E*) E_{V}, idealized THz pulse without any propagation effects. (*F*) $E_{THz}(t)$ pulse halfway in the sample (black line, Eq. **S9**) and for comparison the pulse without any extra phase added (gray line, Eq. **S5**).

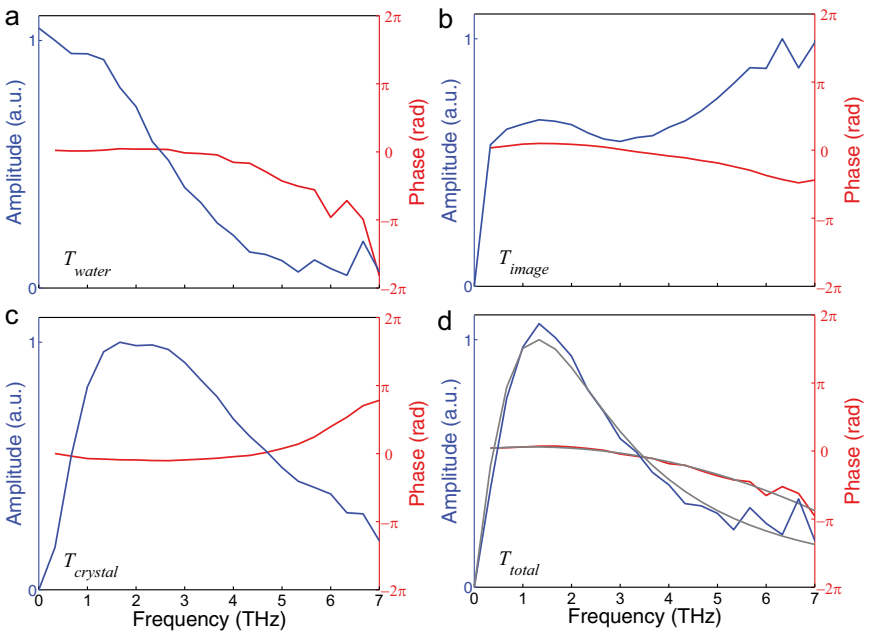

Fig. S5. Transfer functions. (*A*) $T_{water}(\omega)$, (*B*) $T_{image}(\omega)$, (*C*) $T_{crystal}(\omega)$, and (*D*) $T_{total}(\omega)$. The gray lines show the fitted amplitude and phase functions.